VIOBIO Itinerary Planner and Abstract Book

2013 ARVO Annual Meeting

May 04 - 09, 2013

To make changes to your intinerary or view the full meeting schedule, visit http://arvo2013.abstractcentral.com/itin.jsp

Saturday, May 04, 2013

Time	Session Info
8:30 AM-4:30 PM, TCC LL 4/5, **Predicting, Measuring and Treating Changes in Corneal Biomechanics** **SEPARATE REGISTRATION FEE REQUIRED**	
11:50-12:10 PM	**Airpulse OCT** S. Marcos

Sunday, May 05, 2013

Time	Session Info
10:30 AM-12:15 PM, TCC LL 4/5, **Accommodation and Presbyopia**	
10:45-11:00 AM	**382. Three-dimensional biometry and alignment in eyes implanted with Accommodative IOLs as a function of accommodative demand** S. Marcos; S. Ortiz; P. Perez-Merino; M. Velasco; M. Sun; J. Birkenfeld; S. Duran; I. Jimenez-Alfaro

Monday, May 06, 2013

Time	Session Info
8:30 AM-10:15 AM, Exhibit / Poster Hall, **Corneal Cross-linking and Biomechanics**	
8:30 AM-10:15 AM	**1630 - D0265. OCT-Vibrography: A Novel Non-Contact Method to Estimate Corneal Biomechanical Properties** S. Kling; E. Chang; G. Scarcelli; N. Bekesi; S.H. Yun; S. Marcos
8:30 AM-10:15 AM, TCC LL 4/5, **Aberrations, Image Quality and Visual Performance**	
9:00-9:15 AM	**1281. Visual performance under natural, corrected and Adaptive Optics induced astigmatism: meridional and adaptational effects** M. Vinas; P. De Gracia; C. Dorronsoro; L. Sawides; G. Marin; M. Hernandez; S. Marcos

Tuesday, May 07, 2013

You have nothing scheduled for this day

Wednesday, May 08, 2013

Time	Session Info

8:30 AM-10:15 AM, Exhibit / Poster Hall, **Accommodation and Presbyopia Correction**	
8:30 AM-10:15 AM	**4267 - B0304. Contribution of shape and gradient index to the spherical aberration of donor human lenses** J. Birkenfeld; A. de Castro; S. Marcos
8:30 AM-10:15 AM	**4272 - B0309. Lens Spherical Aberration Changes in Cynomolgus Monkeys during Simulated Accommodation in a Lens Stretcher** B.M. Maceo; F. Manns; A. de Castro; S. Uhlhorn; E. Arrieta; S. Marcos; J.A. Parel
8:30 AM-10:15 AM, TCC LL 4/5, **Spatial Vision, Visual Psychophysics and Aging II**	
9:45-10:00 AM	**4068. Optical quality and subjective judgments of blur under pure simultaneous vision** C. Dorronsoro; A. Radhakrishnan; L. Sawides; S. Marcos
8:30 AM-10:15 AM, TCC 303, **Keratoconus and Biomechanics**	
10:00-10:15 AM	**4075. Brillouin microscopy of collagen crosslinking: non-contact depth -dependent analysis of corneal elastic modulus** G. Scarcelli; S. Kling; E. Quijano; R. Pineda; S. Marcos; S.H. Yun

Thursday, May 09, 2013

You have nothing scheduled for this day

Final ID:

Airpulse OCT

S. Marcos; [1];

1. Instituto de Optica, Consejo Sup de Investig Sci, Madrid, Spain.

Final ID: 382

Three-dimensional biometry and alignment in eyes implanted with Accommodative IOLs as a function of accommodative demand

S. Marcos; [1]; *S. Ortiz;* [1]; *P. Perez-Merino;* [1]; *M. Velasco;* [1]; *M. Sun;* [1]; *J. Birkenfeld;* [1]; *S. Duran;* [2]; *I. Jimenez-Alfaro;* [2];

1. Instituto de Optica, Consejo Superior de Investigaciones Cientificas, Madrid, Spain.
2. Fundacion Jimenez Diaz, Madrid, Spain.

Purpose: Accommodative intraocular lenses (A-IOLs) appear as a promising solution for the correction of presbyopia. We used custom spectral Optical Coherence Tomography (sOCT) to fully image and quantify in 3D the anterior segment of the eye in patients implanted with A-IOLs designed to move axially inside the eye.

Methods: Custom sOCT provided with quantification tools (automatic image analysis and fan an optical distortion correction algorithms) was used to fully image in 3D the ocular anterior segment in 20 eyes from 10 patients (73-82 years old) implanted with single-optic A-IOLs (Crystalens AO, B&L). Measurements were performed pre-operatively, and post-operatively for 0, 1.25 and 2.5 D accommodative demands, under phenilephrine. The following parameters were extracted from the images: anterior and posterior corneal and lens (natural and A-IOL) surface 3D geometry, pre-and post- anterior chamber depth (ACD), and lens and A-IOL tilt. ACD and lens alignment were estimated from 3D data, from the distances between surface apices, and from the vectors normal to the pupil and lens planes, respectively.

Results: Data were obtained from fully registered pre/post-operative images, and from images corresponding to different accommodative demands (see Figure). The average ACD pre-op was 2.67±0.25 mm, and post-op (relaxed accommodation) was 3.84±0.39 mm, with high left/right eye symmetry. Most lenses moved axially backward upon an accommodative demand (up to 0.4 mm), opposite from the expected shift by design. Only five lenses moved forward (up to 0.11 mm). Natural lens tilt ranged from -2.14 to 1.84 (superior). The absolute tilt of the implanted A-IOLs was on average higher than the natural lens' tilt; in 5 eyes the A-IOL tilt exceeded by more than x2.5 the pre-op tilt, and changed orientation. A-IOLs tilts generally occurred in the superior/nasal orientation. Most lenses changed tilt with accommodative demand (from 0 to 9 deg/D, on average across eyes).

Conclusions: Quantitative sOCT imaging of the pre- and post-operative anterior segment of the eye appear essential to understand the mechanisms by which current A-IOLs operate and advance towards new developments. The tested A-IOL did not work as expected in most eyes, indicating that potential improvements in near vision are unlikely resulting from effective change in paraxial power, but may be associated to induced lens tilt.

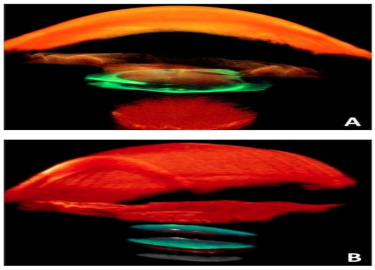

Merged 3D Full anterior segment OCT images of **(A)** a pre-op (with cataract) and post-op (A-IOL) eye; **(B)** post-op eye with A-IOLs for three accommodative demands (green:0 D; red:1.25D; gray: 2.5 D)

Final ID: 1630 - D0265

OCT-Vibrography: A Novel Non-Contact Method to Estimate Corneal Biomechanical Properties

S. Kling; [1]; *E. Chang;* [2]; *G. Scarcelli;* [2]; *N. Bekesi;* [1]; *S. H. Yun;* [2]; *S. Marcos;* [1];

1. Instituto de Optica, Consejo Superior de Invest Cientificas, Madrid, Spain.
2. Wellman Center, Massachusetts General Hospital, Boston, MA, United States.

Purpose: Corneal biomechanics are key for diagnosing corneal pathologies and evaluating treatments that alter corneal geometry or stiffness. Most methods to measure corneal biomechanics are destructive, while in-vivo techniques (e.g. air-puff imaging) are biased by corneal geometry and IOP. We developed a new technique to determine corneal material parameters, while reducing current prevalent restrictions.

Methods: Sound excitation (100-110 db) together with phase sensitive OCT was used to measure the profile of the natural frequencies (range 200-1000 Hz) in corneal tissue. The technique was tested in-vitro on 6 freshly enucleated pig and bovine eyes, using corneal flaps, corneal buttons and whole eyes. Different conditions were tested (virgin, riboflavin-dextran instillation, cross-linking CXL) to determine the effect of corneal rigidity and hydration. Changes in corneal stiffness were determined by the shift of natural frequencies and viscoelastic behavior by the phase lag between sound wave and corneal oscillation. Finite element (FE) models were built to simulate the experimental observations.

Results: We found an experimental shift in the first natural frequency of 101.25±67.1 Hz between the anterior flaps of virgin and CXL corneas; no significant shift was observed for posterior flaps (-12.5±32.0 Hz). Corneal buttons and globes confirmed a frequency shift after cross-linking. The phase lag was sensitive to the tested frequency and to corneal fixation (δ(flap)=4.06, δ (button)=6.19 and δ(globe)= 5.93 at 355Hz). FE-models predicted the first natural frequency to be strongly correlated with corneal stiffness (ΔE=+1.4MPa, Δf(globe)=+100Hz, Δf(button)=+250Hz, Δf(flap)=+150Hz). Natural frequencies of higher modes were also sensitive to IOP, corneal curvature, thickness and density.

Conclusions: OCT vibrography is a promising non-invasive technique for the estimation of corneal biomechanical properties, allowing the separation of corneal stiffness from other parameters.

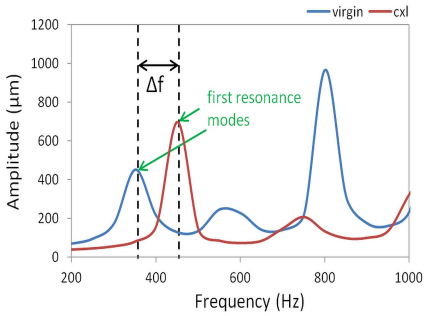

Shift of the first resonance frequency with increased corneal rigidity.

Final ID: 1281

Visual performance under natural, corrected and Adaptive Optics induced astigmatism: meridional and adaptational effects

M. Vinas; [1]; *P. De Gracia;* [1]; *C. Dorronsoro;* [1]; *L. Sawides;* [1]; *G. Marin;* [2]; *M. Hernandez;* [2]; *S. Marcos;* [1];
1. Visual Optics & Biophotonics Lab, Instituto de Optica, CSIC, Madrid, Spain.
2. R&D, Vision Science Department, Essilor International, Saint-Maur, France.

Purpose: To study the extent to what prior adaptation to astigmatism affects visual performance, whether this effect is axis-dependent, and the time-scale effect of potential changes in visual performance in the presence of astigmatism following its correction. To study whether the effect of possible positive interactions of aberrations (astigmatism & coma) on visual performance might be altered after long-term adaptation to correction of astigmatism.
Methods: Measurements of visual acuity (VA) were performed under induction of astigmatism and a combination of astigmatism and coma, while controlling the low and high order aberrations (HOA) of the subject with an Adaptive Optics (AO) system, in 25 subjects classified in 3 groups: non-astigmats, habitually-corrected and uncorrected astigmats. Astigmatism (1.00D) was induced at 3 different orientations: at the natural axis, at the perpendicular orientation, and at 45deg for astigmats, and at 0, 90 and 45deg for non-astigmats. Experiments were also performed with coma (0.41μm at a relative angle of 45deg) combined with the mentioned amount/orientations of astigmatism. VA was measured in a total of 14 different conditions, using an 8-Alternative Forced Choice (8AFC) procedure with tumbling E letters and a QUEST algorithm. Uncorrected astigmats were provided with proper astigmatic correction immediately after the first session. Measurements were performed during 6 months following correction.
Results: In non-astigmats, inducing astigmatism at 90deg, under full AO correction, produced a statistically ($p<0.01$) lower reduction in VA (29%) than at 0 (40%) or 45deg (41%). In astigmats, the lower decrease was for astigmatism induced at the natural axis (24% for corrected astigmats, 28% for non-corrected astigmats). 6-months of astigmatic correction wear did not reduce the insensitivity to astigmatism induction along the natural axis. Visual benefit of adding coma to astigmatism over astigmatism alone improved significantly only in non-astigmats, and only for some orientations of astigmatism.
Conclusions: The impact of astigmatism on VA is greatly dependent on the orientation of the induced astigmatism, even in non-astigmats. Prior experience to astigmatism plays a significant role on visual performance in the presence of both astigmatism and combinations of astigmatism and coma, with a strong bias towards the axis of natural astigmatism.

Final ID: 4267 - B0304

Contribution of shape and gradient index to the spherical aberration of donor human lenses

J. Birkenfeld; [1]; *A. de Castro;* [1]; *S. Marcos;* [1];
1. CSIC-Instituto de Optica, Madrid, Spain.

Purpose: The relative contribution of crystalline lens geometry and gradient index (GRIN) to its spherical aberration (SA) and its age-related changes is unknown. We investigated these relationship using Optical Coherence Tomography (OCT) and Laser Ray Tracing (LRT).
Methods: 11 ex vivo human lenses (22-71 years) from an eye bank were imaged in 3D with a custom OCT to obtain optical path differences. The shape of the lens surfaces was extracted from the images using surface segmentation and Zernike polynomial fitting. The lens power was measured using LRT for 2 and 4-mm pupil diameters. The 3D GRIN was estimated by means of an optimization method based on genetic algorithms (de Castro et al. OE 2010), which searched for the parameters of a 4-variable GRIN model that best fits the distorted posterior lens surface of the lens in 18 different meridians. The SA of the lenses was estimated by computational ray tracing, assuming both a homogeneous index and the estimated GRIN.
Results: Geometrical data of all lenses were reconstructed using 3D OCT images. Anterior radius of curvature and asphericity varied widely across lenses (6.1 to 11.3 mm, and -9.9 to 5.6, respectively), and were rather constant for the posterior surface (mean: 5 mm and -0.3, respectively). Lens power ranged from 34D (younger lens) to 24D (older lens). In 10/11 lens power decreased with pupil diameter, revealing a negative spherical aberration. Lens thickness (ranging from 3.8 to 5.2 mm) increased and mean group refractive index (ranging from 1.392 to 1.407) decreased slightly with age. The reconstructed GRIN showed surface refractive index values between 1.368 and 1.376, nucleus refractive index values between 1.403 and 1.415, and an exponential decay value ranging from 1.8 to 3.4 (axial) and from 1.9 to 5.8 (meridional). The estimated SA (from lens geometry and index) ranged from -0.8 to 0.3 μm for the equivalent refractive index, and from -2.1 to -0.3 μm for the estimated GRIN. SA shifted with age towards less negative values (slope=0.028 μm/yr and 0.022 μm/yr assuming equivalent index or GRIN, respectively).
Conclusions: 3D OCT data and experimental power data of human donor lenses of different ages allowed reconstruction of the lens GRIN and evaluation of external geometry and GRIN contribution to the lens spherical aberration. GRIN shifted the SA towards negative values in all cases and played a role in the age-related shift of SA.

Final ID: 4272 - B0309

Lens Spherical Aberration Changes in Cynomolgus Monkeys during Simulated Accommodation in a Lens Stretcher

B. M. Maceo; [1, 2]; *F. Manns;* [1, 2]; *A. de Castro;* [3]; *S. Uhlhorn;* [1]; *E. Arrieta;* [1]; *S. Marcos;* [3]; *J. A. Parel;* [1, 4];

1. Ophthalmic Biophysics Center, Bascom Palmer Eye Institute, Miami, FL, United States.
2. Biomedical Optics and Laser Laboratory, Department of Biomedical Engineering, University of Miami College of Engineering, Coral Gables, FL, United States.
3. Instituto de Óptica, Consejo Superior de Investigaciones Científicas, Madrid, Spain.
4. Vision Cooperative Research Centre, Sydney, NSW, Australia.

Purpose: To quantify the difference in spherical aberration (SA) of cynomolgus monkey lenses in the accommodated and unaccommodated state.

Methods: A Laser Ray Tracing system (LRT) was used to obtain SA measurements on 2 cynomolgus monkey lenses from 2 donors (4.5 and 6.9 years, PMT= 4 and 26 hours). The tissue was mounted in a chamber filled with Dulbecco's Modified Eagle Medium inside a lens stretcher (Ehrmann et al, Clin Exp Opt, 2008). The lens spherical aberration was measured in the unstretched (accommodated) and stretched (relaxed) state. The LRT delivered 51 equally-spaced parallel rays along the vertical meridian of the lens over a total length of 6mm. A camera mounted on a vertical position stage was placed under the chamber containing the lens to sequentially record the spot corresponding to each individual ray. Spot images were measured at up 12 camera positions along the optical axis covering a range of up to 22mm. The images were processed to determine the centroid of each spot and calculate the corresponding ray height at each camera position. For each camera position, the measured ray heights were plotted as a function of entrance ray height and fit with a 3rd order polynomial: $y = A*x + B*x^3$. The A and B coefficients were then plotted as a function of camera position and a linear fit was performed. The effective focal length and Seidel spherical aberration coefficient were extracted from the fits. A ray-trace analysis showed that the posterior window of the chamber contributes less than 1% error to the SA coefficient. Therefore the contribution of the window to spherical aberration was not corrected for.

Results: The results for the two lenses are summarized in the table below:

Conclusions: Spherical aberration in cynomolgus monkey lenses increases in absolute value with accommodation, as found in human and rhesus monkeys.

	Effective Focal Length (mm)			Power (D)			Spherical Aberration (mm^{-3})		
	Unstretched	Stretched	Change	Unstretched	Stretched	Change	Unstretched	Stretched	Change
Lens 1	23.93	45.90	-21.97	56.20	29.30	26.90	-0.076	-0.054	-0.022
Lens 2	22.95	36.15	-13.20	58.60	37.20	21.40	-0.065	-0.051	-0.014

Final ID: 4068

Optical quality and subjective judgments of blur under pure simultaneous vision

C. Dorronsoro; [1]; *A. Radhakrishnan;* [1]; *L. Sawides;* [1]; *S. Marcos;* [1];

1. Instituto de Optica, CSIC, Madrid, Spain.

Purpose: To compare retinal image quality and subjective image sharpness under pure bifocal simultaneous vision (PSV) across a wide range of addition values.

Methods: Four subjects performed a weighted rank psychophysical experiment to grade (from totally blurred to totally sharp, 0 to 5) the perceptual quality of PSV images. As a control condition, the perceptual quality of purely defocused (PD) images was also assessed. Computer generated images of a face were observed, for 1.5s in random order, through adaptive optics to correct the aberrations of the eye. The PSV images (50/50 energy content) were obtained from the combination of a focused image superimposed to a defocused version of the same image. At least 18 defocus conditions (0-3D) were subjectively ranked (10 repetitions). In addition, optical quality was evaluated as a function of defocus, from the PSV and PD Point Spread Functions (PSF), using the Modulation Transfer Function (MTF) at different frequencies as a metric.

Results: As expected, images without defocus were perceived as sharp (score s=5) in all subjects and conditions. The perceptual weighted rank systematically dropped for PD at a rate of 9.0±4.0 s/D, with the images perceived as completely blurred (s=0) from 0.6 D onwards. PSV images provided a similar decrease as their defocus component increased, in the 0-0.3D range. However, in 3 subjects the score reached a minimum at 0.5D (s=2.1±0.4) and then it was partially recovered back towards sharpness (s=3.5 at 1.2D), remaining stable afterwards. The 4th subject showed a similar trend judging PSV images but without a minimum. The objective simulations predicted the perceptual judgment trends, as well as the differences between judgments of PD and PSV images. MTF@20 c/deg decreased sharply with defocus in PD, but reached a minimum (0.42 at 0.5 D) and recovered a stable level (0.50 from 1.5D) in PSV. Averaged MTFs (15-25 c/deg) provided the most accurate predictions.

Conclusions: As opposed to the common idea that simultaneous vision retinal images (as those found in multifocal contact or intraocular lenses) are severely optically degraded, but later restored in neural processes, we have found a good correspondence between pure subjective perception experiments and pure optical simulations. Although our findings do not preclude for possible effects of neural adaptation, neural effects seem to be secondary in the perceptual judgment of sharpness in PSV.

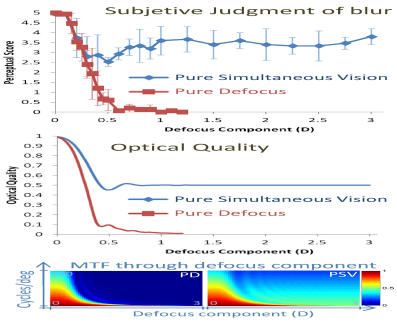

Final ID: 4075

Brillouin microscopy of collagen crosslinking: non-contact depth-dependent analysis of corneal elastic modulus

G. Scarcelli; [1]; *S. Kling;* [2]; *E. Quijano;* [1]; *R. Pineda;* [3]; *S. Marcos;* [2]; *S. H. Yun;* [1];

1. Wellman Center for Photomedicine, Harvard Medical School, Cambridge, MA, United States.
2. Instituto de Optica, Conjejo Superior de investigation cientifica, Madrid, Spain.
3. Ophthalmology, Mass eye and ear Infirmary, Boston, MA, United States.

Purpose: Corneal collagen crosslinking (CXL) is a promising method to treat keratoconus and corneal ectasia. The increase of corneal rigidity produced by CXL is a determinant of treatment outcome. However, it is currently difficult to monitor and objectively evaluate the mechanical outcome due to the lack of suitable methods for measuring the mechanical properties of the cornea in vivo. The objective of this study is to test and validate a recently developed Brillouin microscopy technique for quantifying the corneal mechanical properties before and after CXL.

Methods: CXL was performed on N=21 fresh porcine eyes using various pre-soaking times, light doses, and with (riboflavin-mediated) or without (benzalkonium chloride –mediated) epithelial debridement. A confocal Brillouin microscope was used to measure the Brillouin elastic modulus maps of the corneas without contact before and after CXL. Brillouin corneal stiffness was calculated from the Brillouin cross-sectional maps. The average elastic moduli of anterior, middle, and posterior stromal regions were analyzed for different CXL protocols. Corneal Stiffening Index (CSI) was introduced as a metric to compare the efficacy of a given CXL protocol with respect to the standard Dresden protocol (30-min pre-soak of riboflavin, ultraviolet illumination for 30 min at 3 mW/cm2).

Results: Brillouin corneal stiffness increased significantly ($P<0.001$) by both epi-off and epi-on CXL. The increase of Brillouin modulus was depth-dependent, decreasing from the anterior to posterior regions, indicating that the stiffening of the anterior corneal stroma contributes the most to mechanical changes. The increase of anterior Brillouin modulus was linearly proportional to the light dose. Compared to the standard epi-off procedure, a typical epi-on procedure resulted in a third of stiffness increase (i.e. CSI = 33).

Conclusions: Brillouin microscopy allowed imaging and quantifying CXL-induced changes of elastic modulus, without contact, in a depth-resolved manner, and at a high spatial resolution. This technique may be useful in evaluating the mechanical outcomes of CXL procedures as well as comparing different protocols and CXL agents. This work paves the way towards an objective real-time monitoring of CXL in clinical and in experimental settings.